NO.

ブラジル連邦共和国
パラナベーズン地域
資源開発協力基礎調査報告書

第１年次

平成14年3月

国際協力事業団
金属鉱業事業団

鉱調資
CR(2)
02-055

はしがき

日本国政府はブラジル連邦共和国政府の要請に応え、同国南部に位置するパラナベーズン地域の非鉄鉱物資源賦存の可能性を確認するため衛星画像解析、地質調査などの鉱床探査に関する諸調査を実施することとし、その実施を国際協力事業団に委託した。国際協力事業団は本調査の内容が地質および鉱物資源の調査という専門分野に属することから、調査の実施を金属鉱業事業団に委託することとした。

本調査は平成１３年度から開始された。本年度は第１年次に当たり、金属鉱業事業団は４名の調査団を編成して平成１３年８月１３日から平成１３年１１月２日まで現地に派遣した。現地調査は、ブラジル連邦共和国政府機関の協力を得て予定どおり完了した。

本報告書は、第１年次の調査結果を取りまとめたものである。

終わりに、本調査の実施に当たってご協力頂いたブラジル連邦共和国政府関係機関ならびに外務省、経済産業省、在ブラジル連邦共和国日本国大使館および関係各位の方々に衷心より感謝の意を表するものである。

平成１４年3月

国際協力事業団
総　裁　　川上　隆朗

金属鉱業事業団
理事長　　松田　憲和

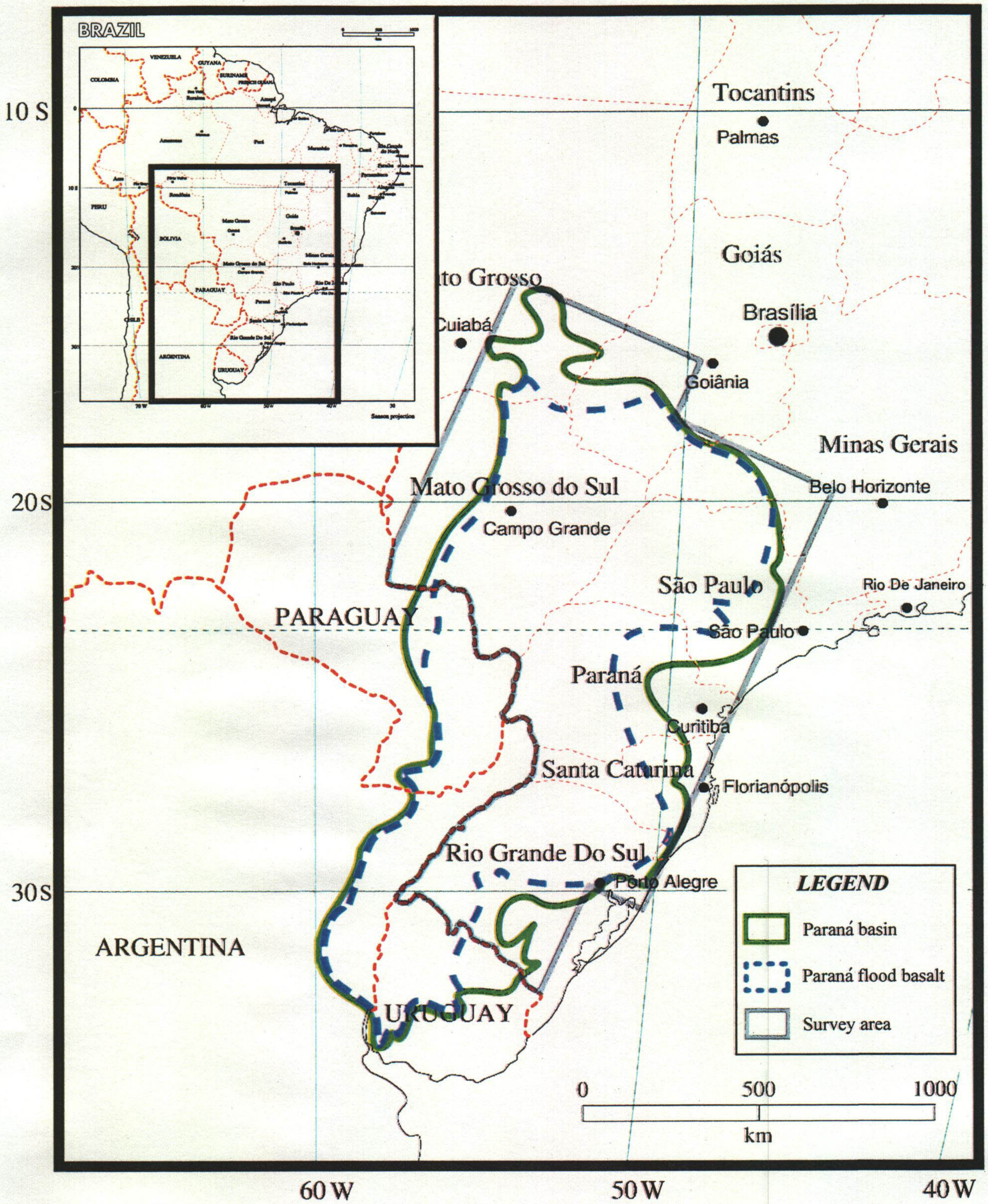

Location of Paraná Basin Area, Brazil

要約

本調査は、ブラジル国と日本国政府との間で平成１３年５月３０日に締結された調査実施実務協定書（Scope of Work）に基づき、同国南東部に位置するパラナ地域において、非鉄金属資源を対象とし、将来、政府間ベースの調査への発展性、あるいは民間企業の新たな調査への参入の可能性を考慮した有望地域抽出を目的として２年間、実施するものである。

第１年次にあたる本年度は、調査地域全域に対して既存データ解析、衛星画像解析および地質調査を実施した。既存データ解析では、洪水玄武岩、Noril'sk 鉱床、パラナベーズンの地質、地質構造および基盤岩の地質、地質構造が、衛星画像解析では JERS-1 の SAR 画像などが解析された。地質調査では主にパラナ洪水玄武岩の全岩分析、微量成分分析および同位体分析などの結果が解析された。

その結果、既存データ解析では、白金属族元素（PGE）の鉱化作用をもたらす洪水玄武岩の起源マグマについて考察された。Noril'sk 鉱床タイプの鉱床生成には、硫黄に不飽和なマグマ、地殻物質の混染作用および大量の珪酸塩マグマとの反応が重要であることが明らかとなった。パラナベーズンのテクトニクスについては高収縮（ε）帯、高重力異常帯、厚いドレライトシル・岩脈の貫入、ベーズン堆積物および洪水玄武岩の層厚変化などから、Paraná 川に沿った NE-SW 方向がリフト（最大圧縮主応力軸 σ_1）、NW-SE 方向がトランスフォーム断層（σ_3）および ENE-WSW 方向がせん断断層帯と推定された。鉱床はこれらの構造方向の交点に形成されているものと解析された。

衛星画像解析では、パラナベーズン中央部を東西方向に横断する範囲を対象にし JERS-1 の SAR データを用いてデジタルモザイク画像を作成し、地質構造の判読・解析を行った。調査地域の面積は約 500,000km^2 で、これをカバーする JERS-1/SAR データ 131 シーンが使用された。調査地域北東部の Ponta Grossa Arch では洪水玄武岩のフィーダーと考えられている多数のドレライト質岩脈群が、明瞭なリニアメントとして抽出された。洪水玄武岩分布域については、地域中央部において NE-SW 方向のまとまったリニアメント群が抽出された。

地質調査では、次のようなことが明らかとなった。パラナベーズン洪水玄武岩類は地化学的特徴から、低 Ti タイプ（Gramado、Esmeralda）、Intermediate タイプ（Paranapanema-Ribiera）および高 Ti タイプ（Pitanga、Urubicí）に分類される。低 Ti タイプの Gramado と Esmeralda は相対的に Th、U、Rb 等の地殻濃集元素を多く含んでいる。高 Ti タイプと Intermediate タイプのマグマはマントル起源のマグマが直接、地表に噴出した可能性が考えられる。Intermediate タイプの Paranapanema-Ribeira の Pt と Pd の平均含有量は最も高い値を示す。この含有量は Noril'sk 鉱床の最も PGE に富んだ溶岩よりも大きい。パラナ洪水玄武岩の化学的な組成から、Noril'sk タイプの正マグマ性硫化物鉱床を生じさせるような PGE 含有量の高いマグマがパラナベーズン地域に存在することが明らかとなった。

EPMA の結果からは、Ponta Grossa Arch と Lomba Grande 地区北東部のシル、岩脈に微量ながら黄銅鉱が含有されることが明らかになった。特に Ponta Grossa Arch のシル、岩脈から微量の閃

亜鉛鉱とニッケルを含有するコバルト砒素鉱物が検出された。

目　次

はしがき
調査地域位置図
要約
目次
図表一覧

第Ｉ部　総論

第１章　序論 1
　１－１　調査実施の経緯 1
　１－２　第１年次調査の概要 2
　　１－２－１　調査目的 2
　　１－２－２　調査地域 2
　　１－２－３　調査方法 2
　　１－２－４　調査団の編成 3
　　１－２－５　調査期間および調査量 3
第２章　調査地域の地理 5
　２－１　位置 5
　２－２　地形 5
　２－３　水系 5
　２－４　気候 5
　２－５　植生 7
第３章　調査地域の地質、鉱床、鉱業事情 8
　３－１　ブラジルの鉱業事情 8
　　３－１－１　鉱業生産 8
　　３－１－２　鉱業政策 9
　　３－１－３　探鉱・開発動向 10
　　３－１－４　最近の鉱業事情 11
　　３－１－５　鉱業関連法規 12
　３－２　ブラジルの地質・鉱床概要 13
　　３－２－１　地質概要 13
　　３－２－２　鉱床概要 23
　３－３　CPRMのPGE国家プログラム 30
　　３－３－１　経緯 30
　　３－３－２　CPRMのプラチナプロジェクトの概要 32
第４章　調査結果の概要 40
　４－１　既存データ解析 40
　　４－１－１　世界の洪水玄武岩の特徴・成因とPGE鉱化作用 40

4－1－2　Noril'sk Cu-Ni-PGE 鉱床とその探査指針 …… 40
4－1－3　パラナベーズンの地質および地質構造 …… 41
4－1－4　大陸性洪水玄武岩に伴う Cu-Ni-PGE 鉱床のテクトニクス …… 42
4－2　衛星画像解析 …… 43
4－3　地質調査 …… 44
第5章　結論および提言 …… 47
5－1　結論 …… 47
5－1－1　既存データ解析 …… 47
5－1－2　衛星画像解析 …… 49
5－1－3　地質調査 …… 49
5－2　第2年次調査への提言 …… 50

第II部　各論

第1章　既存データ解析 …… 53
1－1　収集データの概要 …… 53
1－1－1　学術文献および研究・調査資料 …… 53
1－1－2　地形図 …… 53
1－1－3　地質図 …… 55
1－1－4　空中磁気データ …… 55
1－1－5　GIS データ …… 55
1－2　世界の洪水玄武岩の特徴・成因および PGE 鉱化作用 …… 59
1－2－1　はじめに …… 59
1－2－2　洪水玄武岩の特徴 …… 59
1－2－3　洪水玄武岩の成因 …… 64
1－2－4　洪水玄武岩の成因と PGE 鉱化作用について …… 81
1－3　Noril'sk Cu-Ni-PGE 鉱床とその探査指針 …… 83
1－3－1　はじめに …… 83
1－3－2　地質概要 …… 83
1－3－3　シベリア洪水玄武岩類 …… 88
1－3－4　貫入岩類 …… 91
1－3－5　Noril'sk 鉱床の生成モデル …… 100
1－3－6　正マグマ性硫化鉱物の成因と Noril'sk 型鉱床の探査指針について …… 106
1－4　パラナベーズンの地質および地質構造 …… 114
1－4－1　南米プレートの地質構造区 …… 114
1－4－2　基盤岩の地質および地質構造 …… 119
1－4－3　ベーズンの地質および地質構造 …… 123
1－4－4　地球物理学的データからみた基盤構造 …… 132
1－5　大陸性洪水玄武岩に伴う Ni-Cu-PGE 鉱床のテクトニクス …… 160
1－5－1　Duluth 鉱床 …… 160

１－５－２　Noril’sk鉱床 …… 170
１－５－３　鉱床胚胎の場とテクトニクス …… 177
第２章　衛星画像解析 …… 183
２－１　調査目的 …… 183
２－２　画像処理・作成 …… 183
２－２－１　調査内容 …… 183
２－２－２　対象地域の概要 …… 183
２－２－３　使用衛星データ …… 186
２－２－４　画像処理・作成 ……
２－３　画像判読・解析 …… 187
２－３－１　JERS-1/SAR画像 …… 187
２－３－２　ランドサットTM画像 …… 193
第３章　地質調査 …… 199
３－１　地質概要 …… 199
３－１－１　パラナベーズンの地質概略 …… 199
３－１－２　パラナ洪水玄武岩 …… 202
３－１－３　鉱徴・地化学異常 …… 205
３－２　調査内容 …… 205
３－２－１　試料採集 …… 205
３－２－２　室内試験 …… 209
３－３　パラナベーズンの洪水玄武岩層序 …… 209
３－３－１　化学組成による洪水玄武岩の分類 …… 209
３－３－２　洪水玄武岩の火山層序 …… 228
３－４　パラナ洪水玄武岩類の特徴 …… 232
３－４－１　パラナ洪水玄武岩の地化学的特徴 …… 232
３－４－２　パラナ洪水玄武岩類のPGE含有量について …… 232
３－４－３　地殻物質の混染作用とPGE含有量の関係 …… 235
３－５　MINEROPARによる河川堆積物地化学異常の考察 …… 239
３－５－１　MINEROPARによる沢砂地化学探査について …… 239
３－５－２　地化学異常の要因 …… 239
３－６　洪水玄武岩類に含まれる金属鉱物について …… 246
３－７　沢砂・沢水地化学探査 …… 256
３－７－１　はじめに …… 256
３－７－２　試料の採集および処理 …… 256
３－７－３　調査結果 …… 256
３－７－４　まとめ …… 257
３－８　パラナベーズン縁辺部のマグマ活動とPGEの関係 …… 265
３－８－１　パラナベーズン東縁部における貫入岩体について …… 265
３－８－２　パラナベーズン周辺のアルカリ玄武岩類と周辺の鉱徴地 …… 313
第４章　調査結果の考察 …… 324
４－１　洪水玄武岩の成因論とPGE硫化物鉱床 …… 324

4－2　Noril'sk 鉱床からの Cu-Ni-PGE 鉱床探査指針 ……… 325
4－3　パラナベーズンの地質および地質構造 ……… 325
4－4　大陸性洪水玄武岩に伴う Cu-Ni-PGE 鉱床のテクトニクス ……… 326
4－5　衛星画像解析 ……… 326
4－6　パラナ洪水玄武岩の地化学的特徴 ……… 327
4－7　パラナ洪水玄武岩に関係した貫入岩類 ……… 329
4－8　今後の課題および調査方法 ……… 329

第 III 部　結論および提言

第１章　結論 ……… 331
1－1　既存データ解析 ……… 331
1－2　衛星画像解析 ……… 333
1－3　地質調査 ……… 333
第２章　次年度調査への提言 ……… 335

参考文献および資料 ……… 337

巻末資料

図 表 一 覧

Frontispiece Location of Paraná basin area, Brazil

Figures

Figure I-2-1-1 Location of Paraná basin area, Brazil ······ 6
Figure I-3-2-1 Ages of major tectonic movements and igneous activities in Brazil ······ 15
Figure I-3-2-2 Major old stable continental blocks in Precambrian age of South America ······ 16
Figure I-3-2-3 Directions of orogenic belts in orogenic cycles in Brazil ······ 16
Figure I-3-2-4 Major geological structure sections in Precambrian age in Brazil ······ 18
Figure I-3-2-5 Distribution of sedimentary basins in the Phanerozoic eons in Brazil ······ 19
Figure I-3-2-6 Mesozoic mafic igneous activity in eastern South America (compiled from Rezende, 1972; Bigarella, 1973; McConnelll, 1975; Zamborano & Urien, 1974; Cordani et al., 1967) ······ 22
Figure I-3-2-7 Distribution of aluminum ore deposits and smelting factories ······ 26
Figure I-3-2-8 Distribution of tin ore deposits ······ 27
Figure I-3-2-9 Distribution of Fe/Mn/Cr/Ni/Nb ore deposits ······ 28
Figure I-3-2-10 Distribution of gold and gem stone deposits ······ 29
Figure I-3-3-1 Geological map of Paraná basalt region ······ 31
Figure I-3-3-2 Target areas and bodies for PGE Prospecting by CPRM ······ 36
Figure II-1-1-1 Index map of the topographic maps on a scale of 1/500,000 in the survey area ······ 54
Figure II-1-1-2 Index map of the geological maps on a scale of 1/100,000 made by DNPM - CPRM ······ 56
Figure II-1-1-3 Index map of the airbone magnetic survey ······ 57
Figure II-1-1-4 Index map of the GIS data set ······ 58
Figure II-1-2-1 Global distribution of the major Large Igneous Province (LIP) ······ 61
Figure II-1-2-2 Relationship of the continental breakup and the flood basalts ······ 63
Figure II-1-2-3 Panoramic view of the lava flow in the Deccan Trap (Takahashi and Nakajima, 1997, The photographer: T. Fujii) ······ 65
Figure II-1-2-4 Plots of SiO_2 vs MgO, Al_2O_3 vs MgO, CaO vs MgO and Al_2O_3/CaO ratio vs MgO for Hawaiian lavas (Frey et al., 1994) ······ 68
Figure II-1-2-5 Schematic model of a zoned mantle plume beniath Hawaii (Hauri, 1996) ······ 68
Figure II-1-2-6 Experimentally determined melting characteristics of core (Fe, FeO) and lower mantle material ($MgSiO_3$: perovskite) ······ 70
Figure II-1-2-7 A schematic model of the convection in the mantle ······ 71
Figure II-1-2-8 A schematic model of homogeneous plume head for magma genaration through study of the Columbia River flood basalts ······ 73
Figure II-1-2-9 Volume of plume heads calculated on the basis of McKenzie's model

Figure II-1-2-10 Magma types generated by adiabatic decompression of peridotite (Takahashi, 1996) ········ 74
Figure II-1-2-11 Distribution of the Columbia River basalts and track of the Yellowstone hot spot ········ 75
Figure II-1-2-12 Feature of geochemical composition of the Columbia River flood basalts ········ 75
Figure II-1-2-13 Melting phase relations on the Columbia River basalts listed Table II-1-2-3 (Takahashi et al., 1998) ········ 77
Figure II-1-2-14 Liquidus and solidus for a fertile peridotite (data: Takahashi, 1986) and primitive MORB (data: Yasuda, et al., 1994; Takahashi et al., 1998) under dry condition ········ 79
Figure II-1-2-15 A model for heterogeneous mantle plume head for the initial stage of the Yellowstone hot spot (Takahashi et al., 1998) ········ 79
Figure II-1-3-1 Grades versus production + reserves for major Ni sulfide deposits of the world ········ 85
Figure II-1-3-2 Simplified geologic map of the Noril'sk-Talnakh district (Czamanske et al., 1995) ········ 86
Figure II-1-3-3 Main structural elements of the northwest corner of the Siberian platform (Naldrett, 1992) ········ 87
Figure II-1-3-4 Geologic cross sections of the Noril'sk-Talnakh district platform (Naldrett, 1992) ········ 89
Figure II-1-3-5 Correlation chart relating flood basalt stratigraphy of the Noril'sk region (Czamanske et al., 1995) ········ 90
Figure II-1-3-6 Relation between La/Sm versus Gd/Yb for basalts of the Noril'sk region (Naldrett, 1992) ········ 92
Figure II-1-3-7 Vertical variation in La/Sm, Ni, Cu, Pt for basalts of the Noril'sk region (Naldrett, 1999) ········ 92
Figure II-1-3-8 Generalized stratigraphic column for Silurian to Permian formations based on typical stratigraphic thickness for the Tanlakh ore junction (Czamanske et al., 1995) ········ 93
Figure II-1-3-9 Generalized lithologic section for the "fully differentiated" main body of the ore-forming intrusions (Czamanske et al., 1995) ········ 95
Figure II-1-3-10 A) Projection to the surface of the main body of the NE and SW branch of the Talnakh intrusion (Czamanske et al., 1995); B) Cross section of the thickest part of the NE branch of the intrusion (Czamanske et al., 1995) ········ 96
Figure II-1-3-11 Cross section through the east branch of Noril'sk I intrusion (Naldrett, 1999) ········ 97
Figure II-1-3-12 Composite lithologic section of the Talnakh intrusion (Czamanske et al., 1995) ········ 98

Figure II-1-3-13 Vertical variations in major and trace element for the Talnakh intrusion (Czamanske et al., 1995) ········ 99
Figure II-1-3-14 Evolution of the magmas parental to the Lower Talnakh type and the Noril'sk type ore-bearing intrusions ········ 101
Figure II-1-3-15 (a), (b), (c)

Formation of the Noril'sk type ore-bearing intrusion 102
Figure II-1-3-16 Ni-Cu correlation in lavas from the Noril'sk region 110
Figure II-1-3-17 Ni-Au correlation in lavas from the Noril'sk region 110
Figure II-1-3-18 Ni-Pd correlation in lavas from the Noril'sk region 111
Figure II-1-3-19 Ni-Pt correlation in lavas from the Noril'sk region 111
Figure II-1-3-20 Cu vs. Pd discriminant diagram for lavas from the Noril'sk region between the field of rocks formed by sulfur-saturated magmas and the field of rocks formed by sulfur-undersaturated magmas 112
Figure II-1-4-1 World data set regression line (solid) and the standard deviation (dashed curves) of the calculated Te for 36 stations (M.S.M. Mantvani et al., 2001) 116
Figure II-1-4-2 Effective elastic thickness (Te) pattern of the South American Plate 117
Figure II-1-4-3 South America effective elastic thickness pattern in correspondence with tectonic provinces, seismic activity and the age provinces map of Condie (1982) 118
Figure II-1-4-4 Schematic map of basement and tectonic framework of the Paraná basin (E.J. Milani, 1998) 120
Figure II-1-4-5 Geological and tectonic map around the Paraná basin (modified by Mantovani et al., 1991) 121
Figure II-1-4-6 Principal archs, faults in the Paraná basin (M.C.L. Quintas, 1995) 124
Figure II-1-4-7 Simplified Geological map of the Paraná basin, with tectonic elements and geographic references (E.J. Milani et al., 1995) 125
Figure II-1-4-8 Sequence-stratigraphic chart for the Paraná basin 127
Figure II-1-4-9 Isopach map of the Rio Ivai Sequence (E.J. Milani et al., 1998) 128
Figure II-1-4-10 Isopach map of the Paraná supersequence (E.J. Milani et al., 1998) 130
Figure II-1-4-11 Isopach map of the Gondwana I supersequence (E.J. Milani et al., 1998) 131
Figure II-1-4-12 Occurrence of the Gondwana II supersequence (E.J. Milani et al., 1998) 133
Figure II-1-4-13 Isopach map of the Gondwana III supersequence sediments + volcanics (E.J. Milani et al., 1998) 134
Figure II-1-4-14 Isopach map of the Bauru supersequence (E.J. Milani et al., 1998) 135
Figure II-1-4-15 Genetic models of the intracratonic basin (Bott, 1981) 137
Figure II-1-4-16 Thermomechanical model for formation of intracratonic basin 139
Figure II-1-4-17 Isostatic model of Airy (Karner, 1982)........ 139
Figure II-1-4-18 Locations of drilling holes used by M.C.L. Quintas (1995)........ 142
Figure II-1-4-19 Calculated tectonic subsidences (backstripping method). 144
Figure II-1-4-20 Iso-attenuation map of the first distensible event (440 Ma) (M.C.L. Quintas, 1995) 147
Figure II-1-4-21 Accumulated thickness of sills, modified from Zalan et al, (1986) (M.C.L. Quintas, 1995) 148
Figure II-1-4-22 Iso- attenuation map of the second distensible event after the simulation of erosion (296 Ma) (M.C.L. Quintas, 1995) 149
Figure II-1-4-23 Sense of rupture of Gondwana (Turner et al., 1994) 150

Figure II-1-4-24 Iso-attenuation map of the third distensible event after the simulation of erosion (144 Ma) (M.C.L. Quintas, 1995) ······ 151

Figure II-1-4-25 Bouguer anomaly calculated from observed data (M.C.L. Quintas, 1995) ······ 153

Figure II-1-4-26 Anomaly calculated due to the Paraná basin, considering anomalies generated by sediments, igneous rocks, sills and “root” (M.C.L. Quintas, 1995) ······ 154

Figure II-1-4-27 Gravimetric trend anomaly generated by the second order polynomial (M.C.L. Quintas, 1995) ······ 155

Figure II-1-4-28 Residual anomaly substracted the second order trend anomaly from the Bouguer anomaly indicating zones of major attenuations related with two distensible events (M.C.L. Quintas, 1995) ······ 156

Figure II-1-4-29 Hypothetical model for geotectonic evolution of segments adjacent to Paraguay belt, inferred by geological observations in south western Goias region (extracted from Pimental and Fuck, 1995) ······ 158

Figure II-1-4-30 Tectonic provinces of basement rocks and lineaments inferred form residual gravimetric anomalies (M.C.L. Quintas, 1995) ······ 159

Figure II-1-5-1 Generalized map of the Midcontinent rift of North America, after P.W. Weiblen (1980) ······ 161

Figure II-1-5-2 Generalized map of the Lake Superior region ······ 161

Figure II-1-5-3 Generalized bedrock geological map (A) and the cross section (B) of the Duluth Complex (P.W. Weiblen, 1982) ······ 163

Figure II-1-5-4 Cross section along Fig. II-1-5-3 ······ 164

Figure II-1-5-5 Generalized map view of the Kawishiwi area of the Duluth Complex ······ 164

Figure II-1-5-6 Normalization plots of compositions of Keweenawan dikes and sills; Mid-Ocean Ridge Basalt (MORB), and mantle plume basalt (High-Ti Faeroe Islands basalt) ······ 165

Figure II-1-5-7 Variation diagram of MgO versus TiO_2 for Keweenawan dikes and sills in Minnesota and Michigan ······ 165

Figure II-1-5-8 Formation of aulacogene (b) associated with the rupture of the continent (a) ······ 167

Figure II-1-5-9 Possible analogies between the geometry of the igneous rocks associated with the Tertiary opening of the North Atlantic and those in the Midcontinent Rift System ······ 167

Figure II-1-5-10 Shear mechanisms for producing extensional features in rocks ······ 168

Figure II-1-5-11 Hypothetical transition in tectonic regimes proposed for the Midcontinent Rift System ······ 168

Figure II-1-5-12 Rifting models for the Midcontinent Rift System (from Norman, 1978) ······ 169

Figure II-1-5-13 Regional patterns of geophysical anomalies in the Midcontinent Rift System ······ 169

Figure II-1-5-14 Reconstruction of the position of the American, European, Siberian, Kazakhstan, north China, and several smaller plates ······ 171

Figure II-1-5-15 Diagram of geological geotectonic zoning and the Siberian Continental drift ······ 172

Figure II-1-5-16 Isopach map of thickness of crust, limited by the surface of Mohorovicic and that of the Paleozoic (and is some places Mesozoic) foundation ······ 172
Figure II-1-5-17 Copper deposits and the Siberian fractural structural suture ······ 173
Figure II-1-5-18 Scheme of distribution of traps on the Siberian platform (from data by Lurje and Masaitis, 1964) ······ 173
Figure II-1-5-19 Map of the Norilsk region showing the outcrop of the lavas (areas surrounded by lines with attached hatching), main tectonic elements and principal ore junctions (from Naldrett et al, 1992) ······ 176
Figure II-1-5-20 Thickness of the Nadezhinsky formation (lower+middle+upper) suite which illustrates the basin into which lavas were accumulating at the time of eruption (after Naldrett et al, 1992) ······ 176
Figure II-1-5-21 Plan showing the outline of the Northwest Talnakh intrutions, showing the distribution of lenses of massive sulfide ······ 176
Figure II-1-5-22 Interior structure of crush zone of the shear fracture formed by rock failure test (a) and those of vein (b~d) (K. Otsuki et al., 1991) ······ 178
Figure II-1-5-23 Formation model of Duluth mineralized intrusive complex ······ 178
Figure II-1-5-24 Formation model of Noril'sk ore deposit ······ 179
Figure II-1-5-25 Comprehensive analysis map among the basement structure, basin sediment, gravity anomaly and regional stress field in the Parana basin ······ 181
Figure II-2-2-1 Location map of JERS-1/SAR image analysis ······ 184
Figure II-2-2-2 Flow chert of producing JERS-1/SAR mosaic image ······ 186
Figure II-2-2-3 JERS-1/SAR mosaic image ······ 189
Figure II-2-3-1 Interpretation map based on JERS-1/SAR mozaic image ······ 191
Figure II-2-3-2 Landsat TM mosaic image ······ 195
Figure II-2-3-3 Interpretation map based on Landsat TM mosaic image ······ 197
Figure II-3-1-1 Generalized geological sketch map of Paraná basin (Melfi et al, 1988) ······ 200
Figure II-3-1-2 Sequence-stratigraphic chart for the Paraná basin (simplified from Milani et al., 1974) ······ 201
Figure II-3-1-3 Isopachs of combined sill thicknesses with Paraná basin sediments (Bellieni et al, 1984) ······ 204
Figure II-3-2-1 Distribution of collected samples and Paraná flood basalts ······ 207
Figure II-3-3-1 Distribution of classified lava samples and Paraná flood basalts ······ 215
Figure II-3-3-2 Selected variation diagrams of major elements for lava samples ······ 217
Figure II-3-3-3 Selected variation diagrams of trace elements for lava samples ······ 219
Figure II-3-3-4 Spider diagrams of trace elements for lava samples ······ 220
Figure II-3-3-5 Selected variation diagrams of metallic elements for lava samples ······ 221
Figure II-3-3-6 Plots of Mg# vs La/Sm ratio, Mg# vs Gd/Yb ratio and Mg# vs Nb/Zr ratio for lava samples ······ 223
Figure II-3-3-7 Plots of Ta/Nb ratio vs Y/Nb ratio and Zr/Nb ratio versus Y/Nb ratio for lava samples ······ 224
Figure II-3-3-8 Plots of Ba/Ca vs Sr/Ca for lava samples ······ 225

Figure II-3-3-9 Plots of ^{87}Sr/^{86}Sr ratio and ^{143}Nd/^{144}Nd ratio for lava samples 226
Figure II-3-3-10 Chemical stratigraphy by drill samples along north-south direction in Paraná basin 229
Figure II-3-4-1 Pt-Pd correlation in lavas 234
Figure II-3-4-2 Cu vs. Pd discriminant diagram between the field of rocks formed by Sulphur-saturated magmas and the field of rocks formed by Sulphur-undersaturated magmas 236
Figure II-3-4-3 Th/Nb-Pd (A) and U/Nb-Pd (B) correlations in lavas 238
Figure II-3-5-1 Stream sediment geochemical maps of Ni, Cu, Pt and Pd by MINEROPAR (Lichit, 2000) 240
Figure II-3-5-2 NE-SW trending horst and graben structure by Milani (1997) (Licht, 2000) 240
Figure II-3-5-3 Distribution map of Ni content in lavas 242
Figure II-3-5-4 Distribution map of Cu content in lavas 243
Figure II-3-5-5 Distribution map of Pt content in lavas 244
Figure II-3-5-6 Distribution map of Pd content in lavas 245
Figure II-3-6-1 Microscopic and backscattered electron images (KN022C) 247
Figure II-3-6-2 Microscopic and backscattered electron images (KN033, KN035B) 248
Figure II-3-6-3 Microscopic images (AT03-486 (1)) 249
Figure II-3-6-4 Microscopic and backscattered electron images (AT03-486 (2)) 250
Figure II-3-7-1 Contour map of Ca, Mg, Fe and Si for stream water in Lomba Grande district 258
Figure II-3-7-2 Contour map of Ti, As, SO_4 and Li for stream water in Lomba Grande district 259
Figure II-3-7-3 Contour map of Ba, Th, Cr and Tl for stream water in Lomba Grande district 260
Figure II-3-7-4 Contour map of Co, Ni, Cu and Zn for stream water in Lomba Grande district 261
Figure II-3-7-5 Contour map of Co, Ni, Cu and S for stream sediments in Lomba Grande district 262
Figure II-3-7-6 Contour map of Cr, Ba, Fe and P for stream sediments in Lomba Grande district 263
Figure II-3-8-1 Intrusions studied by the Canada-Brazil cooperative project 266
Figure II-3-8-2 Borehole locations 269
Figure II-3-8-3 Isopach of total thickness of sills 271
Figure II-3-8-4 Isopach of the southeast block 273
Figure II-3-8-5 Isopach of the south block 275
Figure II-3-8-6 Isopach of the north block 277
Figure II-3-8-7 Southeast block bird-eye view 279
Figure II-3-8-8 South block bird-eye view 279
Figure II-3-8-9 Southeast-south block bird-eye view 280
Figure II-3-8-10 North block bird-eye view 280
Figure II-3-8-11 Southeast block A-A' section (scale; 1:250,000, H/V; 1:10) 281
Figure II-3-8-12 Southeast block B-B' section (scale; 1:250,000, H/V; 1:10) 281
Figure II-3-8-13 Southeast block C-C' section (scale; 1:250,000, H/V; 1:10) 283
Figure II-3-8-14 Southeast block D-D' section (scale; 1:250,000, H/V; 1:10) 283
Figure II-3-8-15 South block A-A' section (scale; 1:250,000, H/V; 1:10) 285

Figure II-3-8-16 South block B-B' section (scale; 1:250,000, H/V; 1:10) ········· 287
Figure II-3-8-17 South block C-C' section (scale; 1:250,000, H/V; 1:10) ········· 288
Figure II-3-8-18 North block A-A' section (scale; 1:150,000, H/V; 1:6) ········· 289
Figure II-3-8-19 North block B-B' section (scale; 1:150,000, H/V; 1:6) ········· 290
Figure II-3-8-20 North block C-C' section (scale; 1:150,000, H/V; 1:6) ········· 291
Figure II-3-8-21 North block D-D' section (scale; 1:150,000, H/V; 1:6) ········· 292
Figure II-3-8-22 Mg# - major element diagrams for intrusive rocks ········· 295
Figure II-3-8-23 Mg# - trace element diagrams for intrusive rocks ········· 296
Figure II-3-8-24 Mg# - chalcophile element diagrams for intrusive rocks ········· 297
Figure II-3-8-25 Vertical variations in major and trace-element in sill intersected by drill (AT03) ········· 298
Figure II-3-8-26 Vertical variations in major and trace-element in sill intersected by drill (AT08) ········· 299
Figure II-3-8-27 Vertical variations in major and trace-element in sill intersected by drill (TG95) ········· 300
Figure II-3-8-28 Vertical variations in major and trace-element in sill intersected by drill (TG97) ········· 301
Figure II-3-8-29 Vertical variations in major and trace-element in sill intersected by drill (TG228) ········· 302
Figure II-3-8-30 Vertical variations in major and trace-element in sill intersected by drill (TG62) ········· 303
Figure II-3-8-31 Vertical variations in major and trace-element in sill intersected by drill (TG114) ········· 304
Figure II-3-8-32 Pt - Pd correlation diagram for intrusive rocks ········· 306
Figure II-3-8-33 Cu - Pd discriminant diagram for intrusive rocks between the field of rocks formed by sulphur-saturated magmas and the field of rocks formed by sulphur undersaturated magmas ········· 307
Figure II-3-8-34 Th/Nb - Pd correlation for intrusive rocks ········· 309
Figure II-3-8-35 La/Sm - Gd/Yb correlation for intrusive rocks ········· 310
Figure II-3-8-36 (A): Mg-number - Sr-isotope initial ratio diagram; (B): Mg-number - Nd-isotope initial ratio diagram; (C): Sr-isotope initial ratio - Nd-isotope initial ratio diagram ········· 311
Figure II-3-8-37 Alkaline intrusion distribution in Brazil ········· 314
Figure II-3-8-38 Geological map of Lages district (by Sheibe, 1986) ········· 315
Figure II-3-8-38 (continued)
Legend of geological map of Lages district ········· 316
Figure II-3-8-39 Location of altered area and its surrounding geology (geological distribution is compiled after Sheibe; 1986) ········· 319
Figure II-3-8-40 Schematic sketch of the pit for argillized vein with sulfide minerals at the area in Fazenda do Fortunato Muniz in Lages district, Santa Catalina ········· 320

Tables

Table I-1-2-1 Laboratory test ········ 4

Table I-3-1-1 Production of main minerals of Brazil ········ 8

Table I-3-1-2 Mineral production of main companies of Brazil ········ 9

Table I-3-2-1 Major geological events in the South America ········ 14

Table I-3-3-1 Type of PGE deposits in the world and their reserve and production ········ 33

Table I-3-3-2 Samples already collected and analyzed by CPRM PGE project ········ 35

Table II-1-2-1 Mafic and ultramafic bodies and related sulfide ores ········ 60

Table II-1-2-2 Major flood basalts and continental breakup (White and McKenzie, 1989) ········ 62

Table II-1-2-3 Composition of starting materials of melting experience (Takahashi et al., 1998) ········ 77

Table II-1-2-4 Variety of the magma expected from the heterogeneous mantle plume model ········ 82

Table II-1-2-6 Abundance of some transitional metals in earth and planetary materials (Naldrett, 1989) ········ 82

Table II-1-3-1 Classification of mafic and ultramafic bodies (Naldrett, 1989) ········ 84

Table II-1-3-2 Comparison of PGE reserves in the major Ni-Cu-PGE deposits ········ 86

Table II-1-3-3 Volume percentages of the magmatic rock types in the Noril'sk region (fedorenko, 1994) ········ 90

Table II-1-4-1 Intracratonic basin in the world ········ 136

Table II-1-4-2 Locations of drilling holes (M.C.L. Quintas, 1995) ········ 143

Table II-1-4-3 Basic Parameters used in thermomechanic model (M.C.L. Quintas, 1995) ········ 145

Table II-1-4-4 Ratios of tectonic subsidence and total subsidence with the time ········ 145

Table II-2-2-1 List of JERS-1/SAR data ········ 185

Table II-3-3-1 Classification criteria for basalt magma types (Peate et al.,1992) ········ 213

Table II-3-3-2 Analytical results of major, trace and metal elements for Paraná flood basalts in this survey ········ 214

Table II-3-3-3 Nomenclature scheme for the Paraná magma types, and their relationship to previous groups from the Paraná and Etendeka literature (Peate et al., 1992) ········ 230

Table II-3-3-4 Flood basalt provinces of the last 250 Ma and the estimated ages of stratigraphic boundaries involving significant biotic changes ········ 231

Table II-3-4-1 Platinum and palladium concentrations of lava samples ········ 233

Table II-3-6-1 Samples microscopic observation and for EPMA test ········ 246

Table II-3-6-2 EPMA test for intrusive rocks ········ 251

Table II-3-6-3 Metal mineral analysis from Serra Geral basalt flows by CPRM (1/3), (2/3), (3/3) ········ 253

Table II-3-8-1 Samples collected from intrusive rocks ········ 293

Table II-3-8-2 Sulfur isotopic ratios of intrusive rocks ········ 312

Table II-3-8-3 Comparison of chemical composition between Lages basalts and average of some magma types ········ 317

Table II-3-8-4 X-ray diffraction result of argillized samples ········ 322

Table II-3-8-5 Normative calculation of clay mineral assemblage for Lages argillized rocks ………… 323
Table II-3-8-6 Assay results of bulk and pan concentrated samples at Lages area ………… 323
Table II-4-6-1 Summary of geochemical interpretation ………… 328